Trapdoor viscous remanent magnetization

Karl Fabian[1]

[1]Norwegian University of Science and Technology, Department of Geoscience, S. P. Andersens veg 15a, Trondheim, Norway

ORCID: 0000-0002-3504-3292

Key Points:

- Multidomain viscous remanent magnetization (MD VRM) is dominated by decay into trapdoor potential minima
- Previously inexplicable properties of MD VRM are explained by a quantitative trapdoor VRM theory
- Trapdoor VRM suggests an improved methodology for VRM age determination

Corresponding author: Karl Fabian, karl.fabian@ntnu.no

Abstract

Viscous remanent magnetization (VRM) in multidomain particles still exhibits many puzzling properties deviating from the current theory of VRM, based on Neél's single-domain model of magnetic particles with an almost symmetric double-well potential. In larger magnetic particles experimental evidence indicates that more complex magnetization structures preferentially change from high-energy states to low-energy states with large energy differences, such that VRM is preferentially acquired by directed magnetization changes in strongly asymmetric double-well potentials. Here a statistical model explains how this trapdoor VRM (tVRM) naturally explains the experimental observations of initial-state dependence, time-lag variation, non-linear $\log t$ dependence, and acquisition-decay asymmetry for multidomain VRM. It is discussed how tVRM can be experimentally distinguished from single-domain VRM and how the new theory can help to improve age determination by VRM analysis.

Plain Language Summary

The magnetization of rocks is an important property used to determine the history of the Earth surface and the variation of the Earth magnetic field. It is mostly stored by small magnetite particles, which still are larger than about 500 nm in diameter and are called multidomain (MD) magnetites. If a rock, after its formation, lies at the Earth surface for a long time, its magnetization slowly changes and the remanent magnetization newly acquired is called viscous remanent magnetization (VRM). This VRM is very well understood for magnetite particles below about 150 nm in diameter, but no comprehensive theory so far explains all its experimentally observed properties. Here a statistical model is developed that can explain the experimental facts and helps to understand their physical origin. The new theory allows to theoretically investigate different methods to determine the amount of time a rock was exposed to the Earth magnetic field. This leads to a better understanding of time-temperature relations for VRM, and improves the determination of relocation ages based on VRM.

1 Introduction

Viscous remanent magnetization (VRM) is generated when a rock is exposed to a magnetic field for an extended time (Thellier, 1938). Single-domain (SD) VRM is explained by Neél theory (Néel, 1949b, 1949a), but for more complex magnetization struc-

tures, a comprehensive theory is missing (Dunlop, 1983; Tivey & Johnson, 1984; Moskowitz, 1985; Williams & Muxworthy, 2006). Dunlop (1983) finds that room-temperature (RT) VRM is unexpectedly difficult to erase by heating, and that the viscosity coefficient S increases with time, which is now termed non-log(t) behavior (Halgedahl, 1993; Williams & Muxworthy, 2006). For natural rocks, Kent (1985) confirmed that SD blocking time-temperature relaxation theory(Pullaiah et al., 1975) underestimates thermal demagnetization temperatures in Devonian limestones. Tivey and Johnson (1984) provided extensive experimental data that VRM in MD samples is sensitive to the magnetic history of the samples, and that AF demagnetization decreases, while thermal demagnetization increases the ability of MD samples to acquire VRM. Also, both MD and SD samples are sensitive to zero and weak field storage duration Δt prior to the VRM measurement (Tivey & Johnson, 1984). These effects were confirmed for various samples in subsequent experimental studies (Moskowitz, 1985; Halgedahl, 1993; Muxworthy & Williams, 2006; Williams & Muxworthy, 2006; Yu & Tauxe, 2006).

Moskowitz (1985) distinguishes three main physical processes for these magnetic after-effects:

1. Thermal fluctuations (Dunlop, 1973) with diffusion constants S_a for VRM acquisition and S_d for decay.
2. Diffusion after-effect from relaxation due to vacancy/cation diffusion across energy barriers (Street & Woolley, 1950; Kronmüller et al., 1974).
3. Disaccommodation, with a relaxation equation for magnetic susceptibility.

Moskowitz (1985) concludes that over geologic time, thermal fluctuations dominate VRM because the other two effects have relaxation times below 10 ka.

Central problems for MD VRM theory are the pronounced and universal non-log(t) behavior, and the dependence of VRM acquisition on initial state and on waiting time Δt. Moon and Merrill (1986) studied these effects in terms of asymmetric potentials. Microscopic studies of Halgedahl (1993) and Muxworthy and Williams (2006) found episodic random domain reorganization towards more stable magnetization states. The concept of trapdoor processes in VRM acquisition first occurs in relation to the long-term VRM observations by de Groot et al. (2014). VRM overshooting first occurred in a micromag-

netic study by Fabian and Shcherbakov (2018) and was explained by a statistical theory (Fabian, 2000, 2003).

Improving MD VRM theory is important for Holocene age determination, independent of radionuclides (Heller & Markert, 1973; Borradaile, 1996, 2003; Muxworthy et al., 2015; Berndt & Muxworthy, 2017; Sato et al., 2019). Recent VRM models mathematically modify time-temperature relations to explain observed deviations from Neél theory Sato et al. (2016) suggest a mathematical modification of the time-temperature relation, or design concrete models of MD domain wall jumps Berndt and Chang (2018).

Here, a simplified theory quantifies MD VRM behavior including acquisition, decay, reorientation, and thermoviscous relations. It predicts an exponential decay that cumulatively depletes excited magnetization states of increasingly higher energy barriers, and helps to infer viscous magnetization ages using a new approach that is slightly different from Neél theory.

2 Viscous magnetization in a double well potential

Micromagnetism describes physical magnetization structures as local energy minima (LEM). Viscous magnetization changes through thermal activation across an energy barrier between two LEM states S_1, S_2. In Fig. 1a, energies E_1, E_2, and magnetic moments $\mathbf{m_1}, \mathbf{m_2}$ are denoted relative to energy $E = 0$ and moment $\mathbf{m_B}$ at the energy barrier maximum.

If the probability of being in state S_i is ρ_i, then $\rho_1 + \rho_2 = 1$, and the kinetic equation for the dynamic change of ρ_1 is

$$\tau_0 \, \partial_t \rho_1 \;=\; -\, p_{12}\, \rho_1 + p_{21}\, \rho_2 \;=\; -\,(p_{12} + p_{21})\, \rho_1 + p_{21}. \tag{1}$$

Here τ_0 is the attempt period (≈ 1 ns) and p_{ij} the probability to switch from S_i into S_j during τ_0. For weak fields $\mathbf{B}$, not noticeably changing the magnetization at S_1, S_2 and the saddle-point, Arrhenius equation provides

$$p_{ij} \;=\; \exp - \frac{E_i + \mathbf{m_i B}}{k\,T}.$$

Setting the left hand side of (1) to zero yields equilibrium state density and magnetization

$$\bar{\rho}_1 \;=\; \frac{p_{21}}{p_{12} + p_{21}}, \quad \bar{\mathbf{m}} \;=\; \mathbf{m_1}\, \bar{\rho}_1 + \mathbf{m_2}\,(1 - \bar{\rho}_1).$$

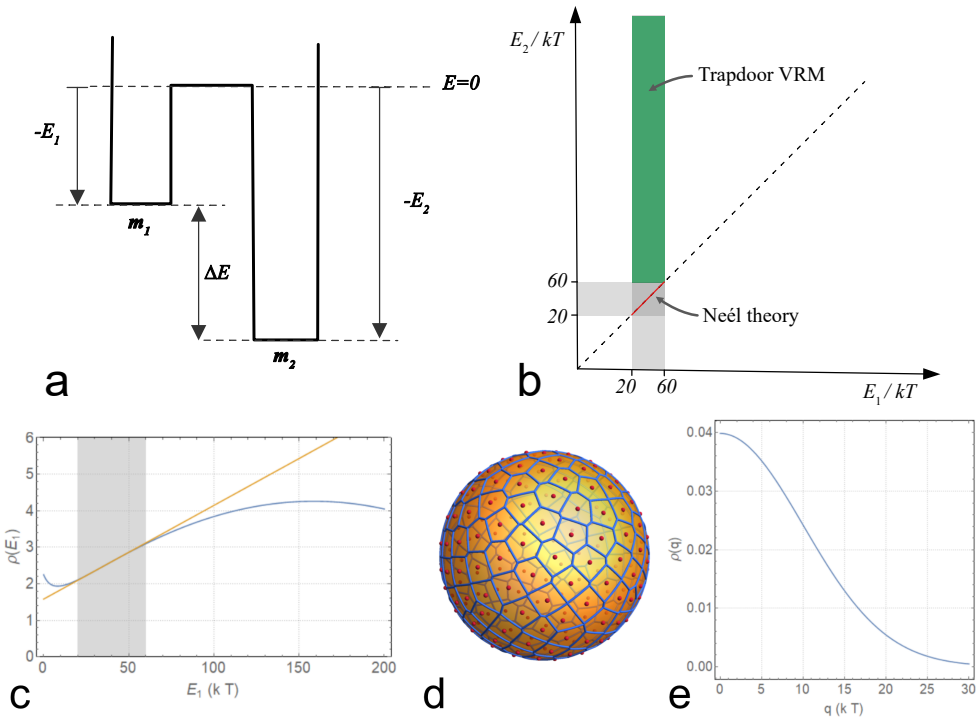

Figure 1. a) Energy barriers between two LEM states with barrier energies $E_1 \leq E_2$. In Neél-theory, the zero-field energies are equal, and the magnetic moments opposite, $E_1 = E_2$, $\mathbf{m_1} = -\mathbf{m_2}$. For trapdoor-VRM theory it is assumed that $E_2 \gg E_1$ and no thermally activated transitions $2 \rightarrow 1$ occur. For an isotropic ensemble it then can be assumed that in the statistical average $\mathbf{m_2} = 0$. b) Range of VRM zero-field energy barriers for Neél theory (red line) and trapdoor VRM (green). c) Approximation of a general energy barrier distribution $\psi_1(w)$ (blue) by a linear function (orange) in the small interval $[w_{\min}, w_{\max}] = [20, 60]$ (gray). d) Representation of the isotropic distribution of magnetic moment directions $\mathbf{u}$ on the sphere by 200 nearly equi-distributed discrete directions (red) with their spherical Voronoi cells (blue). e) Gaussian distribution model of $\psi_3(q)$ for in-field energies $q > 0$ and $\sigma = 10$.

Solving the kinetic equation (1) for the disequilibrium density $\eta = \rho_1 - \bar{\rho}_1$, in time units of τ_0 yields

$$\eta(t) \;=\; \eta_0\, e^{-\lambda\, t}, \tag{2}$$

where

$$\lambda \;=\; p_{12} + p_{21} \;=\; \exp -\frac{E_1 + \mathbf{m_1 B}}{k\,T} + \exp -\frac{E_2 + \mathbf{m_2 B}}{k\,T}$$

is the constant of exponential decay towards $\bar{\rho}_1$. Note, that substituting λ into (2) leads to two nested exponentials which are the primary source of complications when analyzing VRM.

In Neél's theory of SD VRM (sVRM) the micromagnetic energy landscape has only two minima of equal energy $E_1 = E_2$ and opposite magnetic moments $\mathbf{m_2} = -\mathbf{m_1}$. In contrast, trapdoor VRM (tVRM) assumes that E_1 and E_2 are very different, and mathematically corresponds to the limit $E_2 \to \infty$ where

$$\bar{\rho}_1 \;\to\; 0, \quad \lambda \;\to\; \exp -\frac{E_1 + \mathbf{m_1 B}}{k\,T}.$$

By introducing the scaled zero-field barrier $w = E_1/(k\,T)$, the field energy amplitude $q = m\,B/(k\,T)$, and the angular component $\mathbf{u} \cdot \mathbf{b} = \cos\theta$ of the magnetic moment $\mathbf{m_1} = m\,\mathbf{u}$ and the field $\mathbf{B} = B\,\mathbf{b}$, with unit vectors $\mathbf{b}$ and $\mathbf{u}$, the decay constant becomes

$$\lambda \;=\; \exp -(w + q\,\mathbf{u} \cdot \mathbf{b}). \tag{3}$$

3 Theory of trapdoor VRM

The key observation in Neél's theory of SD TRM is that the small range 20-60 of energy barriers E/kT contains all relevant blocking times from the laboratory time scales of about 1 s to geological time-scales of 4 Ga. At RT, only these barriers contribute to VRM acquisition (Fig. 1b).

Only in SD or small pseudo-single domain (PSD) particles do such low barrier energies systematically occur between LEMs with $E_1 \approx E_2$ (red line in Fig. 1b). In larger PSD and MD particles, it is far more likely that for the deeper LEM one has $E_2 \gg 60\; k\,T$ (green area in Fig. 1b), and with overwhelming probability, thermally activated processes only lead from the high-energy state E_1 to the low-energy state E_2. This phenomenon has been compared to a trapdoor in de Groot et al. (2014). A specific example for a trapdoor VRM process is the flower-vortex (F111-V100) transition studied and explained in

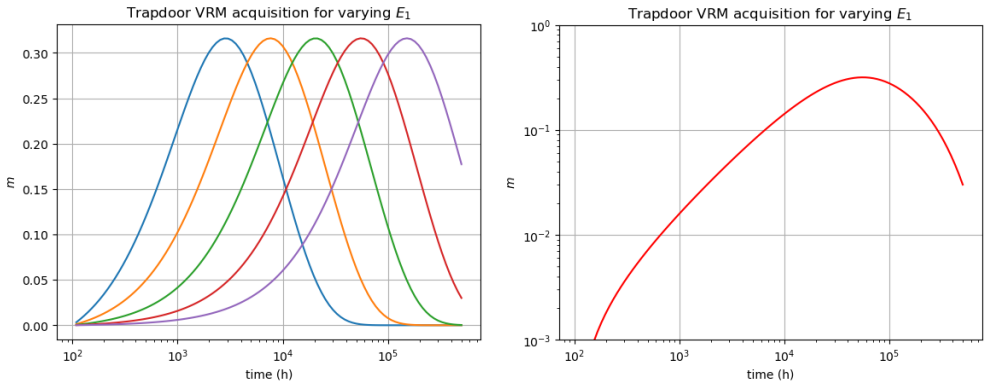

Figure 2. Left: Modeled tVRM acquisition by two oppositely magnetized states $\mathbf{u} \cdot \mathbf{b} = \pm 1$ with $q = 1\,kT$ for different values of $E_1 \in [37, 38, 39, 40, 41]\,kT$ (blue to violet curves). Right: The log-log plot of the left red curve for $E_1 = 40\,kT$ shows nearly linear increase up to about 2×10^4 h (2.3 a) due to the initial depletion of the misaligned states. Only after about 200 a also the aligned states largely are depleted.

Fabian and Shcherbakov (2018) based on micromagnetically calculated energy barriers of a PSD magnetite cube.

While sVRM results from an equilibrium within the current field, tVRM describes an irreversible depletion of high-energy LEMs, where opposite magnetizations with equal zero-field energy decay over different time scales in field. Intermediate tVRM is acquired because field-aligned states become slightly more stable, and their equally probable inverse states decay faster. But once the field-aligned states decayed away, the final tVRM for one value of E_1 is zero. However, new intermediate tVRMs for higher energy barriers are synchroneously acquired, such that the measured VRM over time is dynamically carried by different magnetic moments belonging to increasing energy barriers. Whether this on average increases the measured VRM depends on the sample-specific state-probability distribution and on the initial occupancy of the different LEMs. That an increase in VRM with time is most common is probably due to very long half-lives of misaligned moments for VRM processes with large q.

For example, assume two oppositely magnetized states with $E_1 = 40\,kT$, $q = 1\,kT$, and $\mathbf{u} \cdot \mathbf{b} = \pm 1$. The red curve in Figure 2 displays the VRM acquired and lost by this configuration over time. In the beginning, the states acquire VRM according to a $\log t$ law because the state inverse to the external field with barrier $w - q = 39$ de-

cays first. After 6-7 a the field-aligned states with $w+q = 41$ also decay away and the VRM decreases until after about 100 a it has almost completely vanished. The mathematical similarity of tVRM and radionuclide decay suggests that tVRM also may be useful for age determination.

4 Modeling trapdoor VRM

For quantifying tVRM it is assumed that in the parameter range of interest w, q and $\mathbf{u}$ are statistically independent. The sample specific state-probability density then factors into

$$\psi(w, \mathbf{u}, q) \;=\; \psi_1(w)\, \psi_2(\mathbf{u})\, \psi_3(q).$$

Figure 1c illustrates that the density of zero-field barriers $w = E_1/kT$ on the small interval $[w_{\min}, w_{\max}] = [20, 60]$, can be approximated by a linear state density

$$\psi_1(w) \;=\; \frac{1}{w_{\max} - w_{\min}} + \alpha \left(w - \frac{w_{\max} + w_{\min}}{2} \right).$$

For an isotropic sample, $\psi_2(\mathbf{u})$is constant on the unit sphere. This is numerically modeled by a sufficiently large number of nearly equi-distributed discrete directions on the sphere, each weighted by the area of its Voronoi cell (Fig. 1d). Because the state density $\psi_3(q)$ of the external-field energy q should decay away quickly for large q, it is here modeled by the positive normal distribution

$$\psi_3(q) \;=\; \frac{2}{\sqrt{2\pi}\,\sigma}\, e^{-\frac{q^2}{2\,\sigma^2}},$$

with width σ (Fig. 1e).

The function $\psi(w, \mathbf{u}, q)$ provides the probability for the occurrence of a LEM with parameters $w, \mathbf{u}, q$ in the sample, but not the statistical occupancy of these states, which depends on the magnetic history of the sample. Starting from an initial state occupancy $\rho_0(w, \mathbf{u}, q)$, its evolution is described by

$$\rho(w, \mathbf{u}, q, t) \;=\; \rho_0(w, \mathbf{u}, q)\, \psi(w, \mathbf{u}, q)\, \exp\left(-t\, e^{-(w + q\,(\mathbf{u}\cdot\mathbf{b}))} \right). \tag{4}$$

The numerical models below assume an initially constant state occupancy ρ_0 on the relevant tVRM parameter interval, which approximately represents a thermally demagnetized or a weak field TRM state, assuming that the TRM reflects only a small deviation from the equilibrium absolute zero state. AF demagnetized or ARM states may have different initial state occupancies, where low energy barriers w and larger q states are less

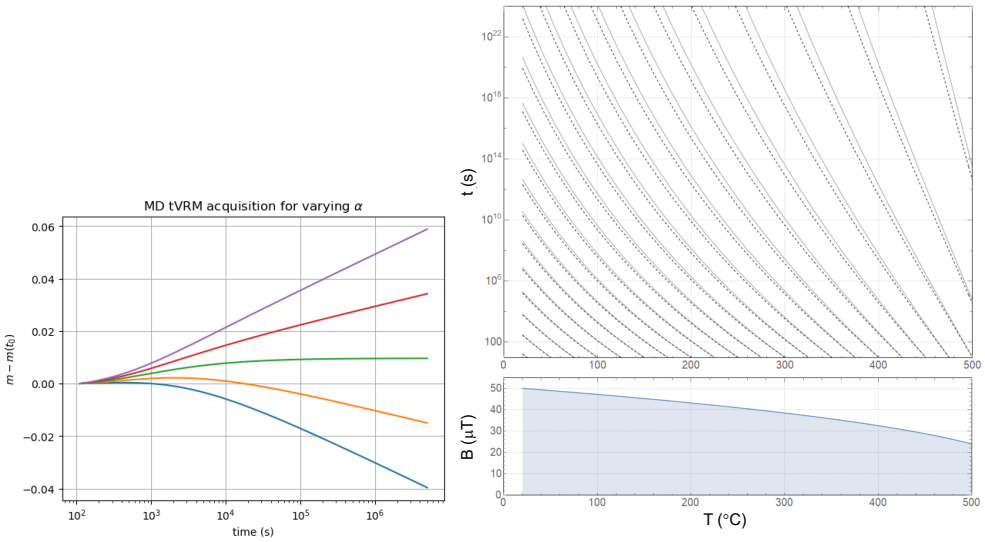

Figure 3. Left: Modeled tVRM acquisition for different values of α in the state-probability $\psi_1(w)$. The shown model uses the parameters $\sigma = 5$, $w \in [20, 80]$ and $\alpha = [-1, -0.5, 0, 0.5, 1]/(w_{max} - w_{min})^2$ for the plots from blue to violet. The model run starts after an initial 500 s VRM acquisition. Note that a decreasing state-probability with increasing w (blue, orange) can lead to decreasing VRM in a positive field, due to the fact that depletion of the field mis-aligned low-w states is not dynamically balanced by larger VRM acquisition of high-w barriers. Right top: Time-temperature diagram for tVRM decay times in MD magnetite calculated using equation (6) for two different critical exponents γ of $M_s(T)$: $\gamma = 0.38$ (solid gray) , $\gamma = 0.36$ (dashed). Right bottom: Required change of applied field as a function of temperature to retain correct tVRM scaling for initial field $B_0 = 50$ μT at RT.

populated than larger w and lower q states. In very old rocks, the 'trapdoor'-components of VRM are already largely activated and trapped in their low-energy minima, such that ρ_0 will be extremely reduced for smaller w.

5 Recovering the tVRM activation history

Because tVRM is a combination of many simple decay processes, to recover the VRM history of a rock, it appears promising to measure which energy levels of LEMs have already been depleted during the time of the rock emplacement. The simplest procedure to measure this would be to again acquire VRM in the same external field for an extended period of time and then identify at what point an increase in VRM acquisition is detected. At this time, new LEM barriers that have not been depleted previously are activated.

Curves like those in Fig. 4 (top right) can then be used to calibrate the experimental data, and infer a viscous-remanence age from the rock.

Unfortunately, VRM of interesting processes was acquired on historical and geological time scales, such that this direct approach is not practical and needs to be replaced by an alternative way to activate higher energy barriers. The classical procedure in Neél theory is to increase the measurement temperature and use time-temperature relations (Pullaiah et al., 1975; Heller & Markert, 1973) to convert between these quantities.

For tVRM acquired by MD magnetite well below the Curie temperature $T_C \approx 580°\mathrm{C}$ the zero-field micromagnetic energy is dominated by the demagnetizing energy which scales with $K_d(T) = \frac{1}{2}\,\mu_0 M_s(T)^2$, such that

$$\frac{E_1(T)}{K_d(T)} \;=\; w\,\frac{k\,T}{K_d(T)}$$

is almost independent of T. Using the saturation magnetization $M_{s,0}$ at 0 K, and the critical exponent $\gamma \approx 0.37$ one has

$$M_s(T) \;=\; M_{s,0}\,(1 - T/T_C)^{\gamma},$$

and with

$$\beta(T) \;=\; \frac{k\,T}{K_d(T)}\frac{K_d(T_0)}{k\,T_0} \;=\; \frac{T}{T_0}\left(\frac{T_C - T_0}{T_C - T}\right)^{2\,\gamma},$$

one can write $w(T) \;\approx\; w\,\beta(T)$. In experiments the same scaling behavior for $q = m\,B$ is achieved by decreasing the applied field strength according to

$$B(T) \;=\; B(T_0)\,\frac{M_s(T)}{M_s(T_0)}. \tag{5}$$

The temperature dependence of the decay constant in (3) is then

$$\lambda(T) \;=\; \lambda^{\beta(T)}.$$

If at temperature T, the laboratory decay time $t_L = 1/\lambda(T)$ activates the same energy barriers as a RT decay time of $t = 1/\lambda(T_0)$ one gets

$$\frac{\log t/\tau_0}{\log t_L/\tau_0} \;\approx\; \frac{1}{\beta(T)}.$$

For $t_L = 10$ s one has $\log t_L/\tau_0 = 23$ with the time-temperature relation

$$\log t/\tau_0 \;\approx\; 23\,\frac{T\,M_s^2(T_0)}{T_0\,M_s^2(T)}. \tag{6}$$

This agrees with the time-temperature relation derived from Neél theory for pure shape anisotropy (Pullaiah et al., 1975), because also in this case only demagnetizing energies are considered. Yet, equation (6) applies to different magnetization processes where the laboratory field is aligned with the natural VRM overprinting field and changes according to the scaling (5). The cumulative depletion of high-energy LEMs generates a substantially different magnetization behavior than the predictions based on Neél theory, although also in the sVRM case for magnetite, VRM at elevated temperatures should be acquired in the correctly scaled field $B(T)$.

Fig. 3(right) demonstrates that this relation predicts a sensitive dependence of tVRM acquisition on temperature and heating rate. Using thermal tVRM acquisition as a dating tool therefore requires very careful experiments allowing for accurate control of the measurement conditions in terms of temperature, measurement time, and thermal equilibration.

In the supplementary material the Python code for a numerical model is provided that allows to simulate arbitrary time-temperature and field histories for magnetite MD ensembles based on the assumption of initially nearly constant probability density.

If the magnetization of a rock was displaced from an initial orientation $\mathbf{m_A}$ to a new orientation $\mathbf{m_B}$ it starts to realign it VRM with the current field H.

6 Discussion

The tVRM model describes a depletion of LEM states with elevated energy by means of a decay equation, and appears simpler than Neél's sVRM theory. What complicates the tVRM model, is the statistical decoupling of magnetic moment vectors and energy barriers. The corresponding evolution of $\rho(w, \mathbf{u}, q, t)$ naturally explains the experimentally observed deviations of MD VRM from Neél theory. The modeling of tVRM is complex, because the integration over the decay equations for all energy barriers and magnetic moments cannot be done analytically and requires numerical treatment. The most notable property of tVRM is that it statistically approaches zero as depicted in Fig. 2, whilst sVRM attains a non-zero equilibrium. The visible tVRM is carried by changing magnetic moments from successively increasing energy barriers. Accordingly, the VRM magnetization curves depend on the distribution and initial occupation of these energy barriers. In Fig. 3(left) the dependence of the slope of the tVRM acquisition curves on

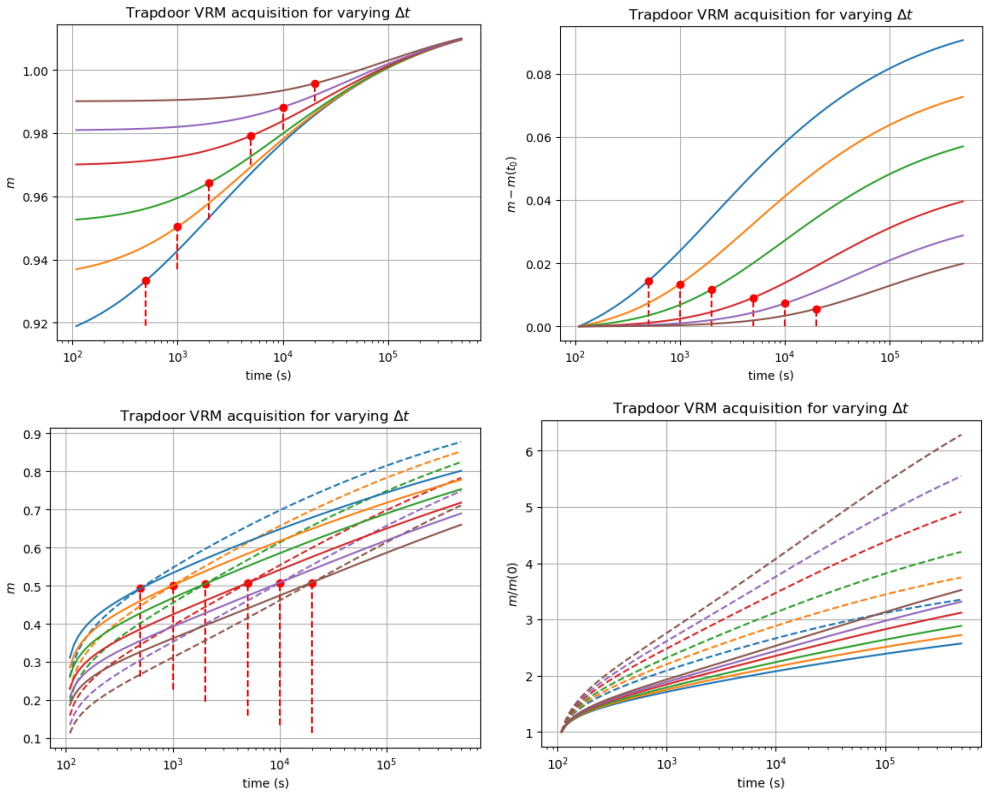

Figure 4. Top left: Modeled tVRM acquisition in an MD sample with initial density defined by $\alpha = 0$, $\sigma = 10$ and VRM acquisition in x-direction for $\Delta t = 0.5, 1, 2, 5, 10, 20 \times 10^3$s (sequence blue to brown). The plot shows the results of a repeated VRM acquisition in x-direction after this history. Note the marked non-log(t) behavior and the systematic dependence on the previous Δt marked by red dots. Top right: The same data after subtracting the initial magnetization to simplify comparison to experiments. Bottom Left: Same as top left, but with initial density after VRM in zero field (dashed lines) or in perpendicular y-direction (solid lines) for $\Delta t = 0.5, 1, 2, 5, 10, 20 \times 10^3$s (sequence blue to brown). Bottom right: The same data as on the left after subtracting the initial magnetization.

the slope α of the zero-field energy distribution $\psi_1(w)$ is plotted. The results demonstrate that tVRM acquired in a positive field may even decrease with time. To what extent details of the distributions ψ_1 and ψ_3 systematically depend on grain size, shape or other average quantities of the magnetic particle ensemble is unclear and requires further study, preferably by micromagnetic models (Conbhuí et al., 2018; Fabian & Shcherbakov, 2018).

A significant deviation from Neél theory is that MD VRM acquisition strongly depends on initial state. sVRM usually starts from a near equilibrium of two equal zero-field energy states, and evolves towards an only slightly different equilibrium. In contrast, tVRM is a pure depletion process modified by the external field. Figure 4 displays model runs which demonstrate that tVRM acquisition depends strongly on the initial population of the high-energy LEMs. The top row shows tVRM acquisition curves after a previous tVRM acquisition in the same direction, that partly depleted the low-w states with field-aligned magnetic moments. tVRM during a second acquisition in the same direction depends on the degree of the first depletion and leads to s-shaped acquisition curves, resembling various experimental results, for example in figures 4,6,7 of (Moskowitz, 1985), figure 2 in (Bikova & Igoshin, 1985), and figures 1,8 in (Lowrie & Kent, 1978).

High activation energy during AF demagnetization of MD samples leads to a lower occupation probability of low-w LEMs than thermal demagnetization. This explains why AF or ARM states in MD samples acquire less VRM than thermally demagnetized or TRM states.

The tVRM model calculations can show both, marked non-$\log t$ behavior and straight $\log t$ behavior, at least over extended time intervals. Non–$\log t$ behavior typically results from partly depleted initial states, where over long time-scales larger energy barriers are activated, that block LEMs with higher occupation probability. Another source of non-$\log t$ behavior can be strongly varying energy barrier distributions in the active region. For tVRM the physical origin of the magnetic energy barrier is irrelevant for the statistical behavior of the sample, such that also diffusion after-effects from vacancy or cation diffusion (Street & Woolley, 1950; Kronmüller et al., 1974) and disaccommodation processes (Moskowitz, 1985) are described by the tVRM model. On some time scales these effects may substantially increase the energy barrier density.

The waiting time Δt effect in principle occurs even for the simple $\log t$-law

$$M(t) - M_0 \;=\; S \log t, \quad \text{for } t > t_0,$$

because it predicts a VRM

$$M_{\Delta t}(t) \;=\; M(t+\Delta t) - M(\Delta t) \approx M(t) - S\,\log(\Delta t),$$

that shows a 'hardening effect' (Dunlop, 1983) due to the asymptotic downward shift $S\,\log\Delta t$. The tVRM model predicts a a strong Δt effect due to the irreversible depletion of LEMs in contrast to the reversible equilibrium shift in the sVRM model. This is leads to a systematic variation in Fig. 4 which contains plots of modeled tVRM acquisitions after different previous acquisition periods Δt.

6.1 Combinations of sVRM and tVRM

In samples with different magnetic grain size populations, both types, sVRM and tVRM, may be present in various combinations. Especially for age determination, it is of interest to separate these two components into

$$VRM \;= sVRM + tVRM.$$

To design methods to identify the more reversible behavior of sVRM is the aim of future experimental studies. The region in Fig. 1b off the red diagonal, where both asymmetric barriers are below 60 $k\,T$ may require separate treatment in certain narrow PSD particle ensembles. This requires the more comprehensive but also more complex Markov chain methods (Fabian & Shcherbakov, 2018). The simpler theory of tVRM focuses on MD particle ensembles, and on ensembles with large grain size variation.

The observation that isothermal VRM is overly difficult to erase by heating (Dunlop, 1983; Kent, 1985) finds a natural explanation in tVRM, where a magnetic moment is almost impossible to move back from a trapped state. To erase such a tVRM with barrier $w{-}q$ it is necessary that the field-aligned magnetizations with their larger in-field barrier $w{+}q$ or zero-field barrier w also decay into their trapped states, which requires higher temperatures than expected for a $w-q$ barrier.

Because tVRM results from a dynamic decay that depletes the occupation probabilities for successively larger energy barriers w, those low-w LEMs that have been depleted cannot be easily occupied again. It is therefore possible to experimentally determine the degree of depletion, and from that infer the time it took to reach this state of depletion. To do this one has to find a measurable difference between depleted and occupated LEMs, which naively can be done by simply repeating the VRM acquisition in

the same external field, and wait until an accelerated tVRM acquisition is observed. Of course, waiting times of thousands of years are unpractical, and thus the time-temperature relation (6) can be used to replace waiting time through measurements at elevated temperatures. To keep the correct scaling, the applied field strength in these measurements must be scaled down, according to (5). Calibration curves for such dating methods, could be developed based on the here presented programs and additional rock magnetic measurements that constrain the LEM state-distribution function ψ.

If tVRM prevails in a rock sample, its VRM acquisition depends strongly on the initial occupation and state-densities ρ_0, ψ, and there exists little reliable data to realistically constrain these functions. Thus, the tVRM concept provides a new incentive and guideline to design targeted experimental and micromagnetic studies to determine realistic density distributions ψ_1 and ψ_3. This will enable a better understanding of VRM processes, improve existing and help to develop new methods of age determination, either directly based on tVRM, or by better isolating the contribution of sVRM.

7 Open Research

The Python code used to model the VRM processes is available in the supporting information. If requested, the code will eventually be deposited at the NTNU repository (dataverse.no) by the time the article is accepted.

Acknowledgments

References

Berndt, T., & Chang, L. (2018). Theory of stable multi-domain thermoviscous remanence based on repeated domain-wall jumps. *Journal of Geophysical Research: Solid Earth*. doi: 10.1029/2018jb016816

Berndt, T., & Muxworthy, A. R. (2017). Dating Icelandic glacial floods using a new viscous remanent magnetization protocol. *Geology*, *45*(4), 339–342. doi: 10.1130/g38600.1

Bikova, E., & Igoshin, L. (1985). On the interrelation between magnetic viscosity and the compositions of magnetites in the alkali-ultrabasic rocks the Kola peninsula. *Izvestiya. Earth Phys.*, *21*, 794-800.

Borradaile, G. J. (1996). An 1800-year archeological experiment in remagnetization. *Geophysical Research Letters*, *23*(13), 1585–1588. doi: 10.1029/96gl01575

Borradaile, G. J. (2003). Viscous magnetization, archaeology and Bayesian statistics of small samples from Israel and England. *Geophysical Research Letters*, *30*(10), 4. doi: 10.1029/2003gl016977

Conbhuí, P. Ó., Williams, W., Fabian, K., Ridley, P., Nagy, L., & Muxworthy, A. R. (2018). MERRILL: Micromagnetic earth related robust interpreted language laboratory. *Geochemistry, Geophysics, Geosystems*, *19*. doi: 10.1002/2017gc007279

de Groot, L. V., Fabian, K., Bakelaar, I. A., & Dekkers, M. J. (2014). Magnetic force microscopy reveals meta-stable magnetic domain states that prevent reliable absolute palaeointensity experiments. *Nature Communications*, *5*.

Dunlop, D. J. (1973). Theory of the magnetic viscosity of lunar and terrestrial rocks. *Reviews of Geophysics*, *11*(4), 855. doi: 10.1029/rg011i004p00855

Dunlop, D. J. (1983). Viscous magnetization of 0.04–100 μm magnetites. *Geophys. J. R. astr. Soc.*, *74*(4), 667–687.

Fabian, K. (2000). Acquisition of thermoremanent magnetization in weak magnetic fields. *Geophysical Journal International*, *142*(2), 478-486.

Fabian, K. (2003). Statistical theory of weak field thermoremanent magnetization in multidomain particle ensembles. *Geophysical Journal International*, *155*(2), 479-488.

Fabian, K., & Shcherbakov, V. P. (2018). Energy barriers in three-dimensional micromagnetic models and the physics of thermoviscous magnetization. *Geophysical Journal International*, *215*(1), 314–324. doi: 10.1093/gji/ggy285

Halgedahl, S. L. (1993). Experiments to investigate the origin of anomalously elevated unblocking temperatures. *Journal of Geophysical Research: Solid Earth*, *98*(B12), 22443–22460. doi: 10.1029/92jb02532

Heller, F., & Markert, H. (1973). The age of viscous remanent magnetization of Hadrian's Wall (Northern England). *Geophysical Journal International*, *31*(4), 395–406. doi: 10.1111/j.1365-246x.1973.tb06510.x

Kent, D. V. (1985). Thermoviscous remagnetization in some Appalachian limestones. *Geophysical Research Letters*, *12*(12), 805–808. doi: 10.1029/gl012i012p00805

Kronmüller, H., Schützenauer, R., & Waltz, F. (1974). Magnetic aftereffects in magnetite. *Phys. Stat. Sol. (a)*, *24*, 487-494.

Lowrie, W., & Kent, D. (1978). Characteristics of VRM in oceanic basalts. *J. Geophys.*, *44*, 297-315.

Moon, T., & Merrill, R. T. (1986). A new mechanism for stable viscous remanent magnetization and overprinting during long magnetic polarity intervals. *Geophysical Research Letters*, *13*(8), 737–740. doi: 10.1029/gl013i008p00737

Moskowitz, B. M. (1985). Magnetic viscosity, diffusion after-effect, and disaccommodation in natural and synthetic samples. *Geophysical Journal International*, *82*(2), 143–161. doi: 10.1111/j.1365-246x.1985.tb05133.x

Muxworthy, A. R., Williams, J., & Heslop, D. (2015). Testing the use of viscous remanent magnetisation to date flood events. *Frontiers in Earth Science*, *3*. doi: 10.3389/feart.2015.00001

Muxworthy, A. R., & Williams, W. (2006). Observations of viscous magnetization in multidomain magnetite. *Journal of Geophysical Research*, *111*(B1). doi: 10.1029/2005jb003902

Néel, L. (1949a). Influence des fluctuations thermiques sur l'aimantation de grains ferromagnétiques très fins. *J. Phys. Sér. B*, *228*, 664-666.

Néel, L. (1949b). Théorie du traînage magnétique des ferromagnétiques en grains fins avec applications aux terres cuites. *Ann. Géophys.*, *5*, 99-136.

Pullaiah, G., Irving, E., Buchan, K., & Dunlop, D. (1975). Magnetization changes caused by burial and uplift. *Physics of the Earth and Planetary Interiors*, *28*, 133-143.

Sato, T., Nakamura, N., Goto, K., Kumagai, Y., Nagahama, H., Minoura, K., ... Roberts, A. P. (2019). Dating of tsunami boulders from Ishigaki Island, Japan, with a modified viscous remanent magnetization approach. *Earth and Planetary Science Letters*, *520*, 94–104. doi: 10.1016/j.epsl.2019.05.028

Sato, T., Nakamura, N., Nagahama, H., & Minoura, K. (2016). Stretched exponential relaxation of viscous remanence and magnetic dating of erratic boulders. *Journal of Geophysical Research: Solid Earth*, *121*(11), 7707–7715. doi: 10.1002/2016jb013281

Street, R., & Woolley, J. C. (1950). Time decrease of magnetic permeability in alnico. *Proceedings of the Physical Society. Section A*, *63*, 509–519.

Thellier, E. (1938). Sur l'aimantation des terres cuites et ses applications géophysiques. *Ann. Inst. Phys. Globe*, *16*, 157-302.

Tivey, M., & Johnson, H. P. (1984). The characterization of viscous remanent magnetization in large and small magnetite particles. *Journal of Geophysical Research*, *89*(B1), 543. doi: 10.1029/jb089ib01p00543

Williams, W., & Muxworthy, A. R. (2006). Understanding viscous magnetization of multidomain magnetite. *Journal of Geophysical Research: Solid Earth*, *111*(B2B02102), B02102. doi: 10.1029/2005jb003695

Yu, Y., & Tauxe, L. (2006). Acquisition of viscous remanent magnetization. *Physics of the Earth and Planetary Interiors*, *159*(1–2), 32–42. doi: 10.1016/j.pepi.2006.05.002